XV International Conference on Computational Plasticity. Fundamentals and Applications
COMPLAS 2019
E. Oñate, D.R.J. Owen, D. Peric, M. Chiumenti & Eduardo de Souza Neto (Eds)

NUMERICAL THERMO-ELASTO-PLASTIC ANALYSIS OF RESIDUAL STRESSES ON DIFFERENT SCALES DURING COOLING OF HOT FORMING PARTS

S. UEBING, L. SCHEUNEMANN, D. BRANDS AND J. SCHRÖDER

Institute of Mechanics, Departement of Civil Engineering
University Duisburg-Essen, Campus Essen
45141 Essen, Germany
e-mail: sonja.uebing@uni-due.de, web page: http://www.uni-due.de/mechanika

Key words: Residual stresses, Multiscale simulation, FE^2-method, Multi-Phase-Field method, Austenite-to-martensite transformation

Abstract. In current research, more and more attention is paid to the understanding of residual stress states as well as the application of targeted residual stresses to extend e.g. life time or stiffness of a part. In course of that, the numerical simulation and analysis of the forming process of components, which goes along with the evolution of residual stresses, play an important role. In this contribution, we focus on the residual stresses arising from the austenite-to-martensite transformation at microscopic and mesoscopic level of a Cr-alloyed steel. A combination of a Multi-Phase-Field model and a two-scale Finite Element simulation is utilized for numerical analysis. A first microscopic simulation considers the lattice change, such that the results can be homogenized and applied on the mesoscale. Based on this result, a polycrystal consisting of a certain number of austenitic grains is built and the phase transformation from austenite to martensite is described with respect to the mesoscale. Afterwards, in a two-scale Finite Element simulation the plastic effects are considered and resulting residual stress states are computed.

1 INTRODUCTION

In the works of [1], [2] and [3], the benefits from hot forming processes in course of generating targeted residual stress states have been established in research. Subsequent heat treatment leads to predefined properties of the component, see [4]. In contrast, specific cooling starting from the forging heat offers the opportunity to adjust material parameters, such as the deformation state, the temperature profile or cooling media, cf. [5]. During such or similar forming processes, residual stresses occur in the material. The classification of residual stresses in three different types relies on [6]. There, the characterization follows the scale under observation. Thus, residual stresses of first type correspond to the complete component and are referred to as macroscopic. Residual stresses of second and third type are in equilibrium concerning the microstructure of the

component, i.e. stresses of second type distinguish between the mean stress of a grain and stresses of first type. Sstresses of third type show location-dependent deviations of the stresses within the grain and the sum of first and second type. Hence, residual stresses of second and third type can be called microscopic.

In the last decades, residual stresses in a component, which result from the forming process, were often minimized or even canceled out to avoid undesired influence on the final properties regarding, for example, lifetime. But in current research, desired effects of residual stress states are targeted, such as enhanced fatigue life, see [7]. Since it is possible to influence the behavior of components decisively, for example with regard to distortion or wear behavior, the overall aim of the paper is to analyze the development of microscopic residual stresses during cooling of hot formed parts.

On that, the computational approach proposed in [8] is followed, where the combination of a Multi-Phase-Field (MPF) model and a two-scale Finite Element (FE) simulation is used. The MPF model enables the numerical computation of different physical phenomena during phase transformations, in general. The theory was introduced by [9], [10] and [11], among others. An advantage of such MPF models in contrast to dual phase-field models is to describe martensitic transformation or grain growth. Furthermore, it is possible to consider an arbitrary number of phases, which differ from each other by e. g. lattice orientation or material properties. It is possible to calculate elastic stresses as well as thermodynamic quantities in terms of phase transformations. Thus, following [12] and [13], the austenite-to-martensite (A-M) phase transformation, which occurs during rapid cooling, can be investigated. Further approaches and application of MPF models can be found in [14], [15] and [16], which analyze elastic modelling of crack growth, while plastic effects are included in [17] and [18] and a viscoplastic material is used in [19]. Additionally, elastic and plastic models for the A-M phase transformation in connection to crack growth have been formulated in [20] and [21].

Afterwards, the two-scale FE simulation is utilized to consider effects of elastic and plastic strains, see e.g. [22] or [23]. Such multiscale approaches provide the opportunity to describe the macroscopic behavior of materials depending on properties of mesoscale or microscale. Thus, thermal anisotropy or microstructural heterogeneity can be expressed. For example, in [24] an approach to consider microstructural graded properties due to A-M transformation in a two-scale simulation has been proposed.

Within the scope of this publication, the model for the computation of mesoscopic residual stresses presented in [8] is used. Therefore, section 2 describes the macroscopic experimental setup and additional simulations, which provides necessary data for the investigation on lower scales. In section 3, a combination of a MPF and a FE simulation is utilized to describe the A-M phase transformation due to cooling and to calculate related residual stresses. Afterwards, section 4 concludes the paper and gives an outlook.

2 MACROSCOPIC EXPERIMENTS AND SIMULATIONS

The numerical analysis of the evolving residual stresses on minor scales depends on macroscopic data which is obtained during the work on the project “Experimental and numerical modeling and analysis of microstructural residual stresses in hot bulk forming

parts under specific cooling" as part of the DFG priority program SPP 2013. This section introduces briefly the experimental set up as well as related macroscopic simulations. For further details, the interested reader is referred to [8].

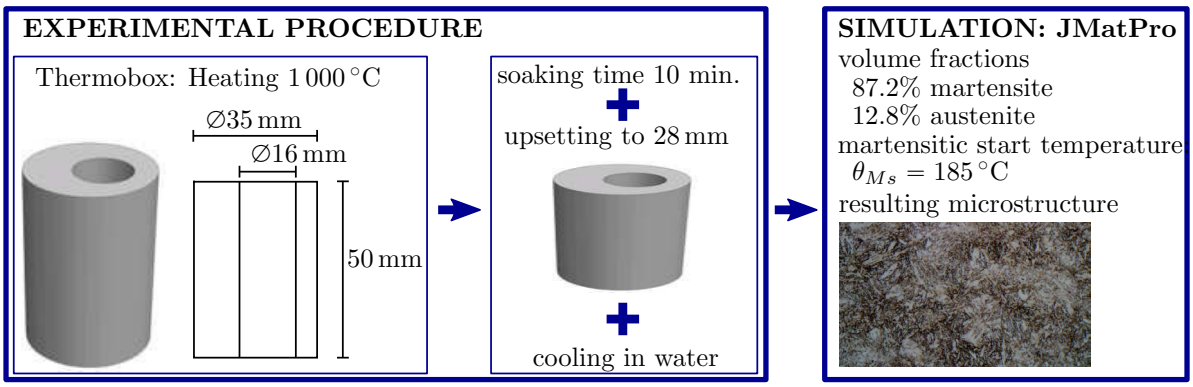

Figure 1: Experimental procedure of upsetting test for a cylindrical specimen and the related macroscopic Finite Element simulation with JMatPro.

The considered specimen, shown in figure 1, is a cylinder made of steel alloy 1.3505 (DIN 100Cr6). Its inital height is 50 mm and the outer diameter equals 35 mm. A hole with a diameter of 16 mm and an eccentricity of 3.5 mm are chosen according to [25], since thereby inhomogeneous residual stress states can be expected. Firstly, the cylinder is heated up to 1 000 °C in a thermobox, such that a stress free austenitic state is formed. After a suitable soaking time of ten minutes, the specimen is upset to a height of 28 mm, still exhibited to the high temperature, before it is rapidly cooled in water. Thus, a diffusionless phase transformation occurs, which results in a martensitic, body-centered tetragonal lattice structure.

In addition to the experiments, the thermodynamic simulation software JMatPro [26] provides further material data based on the chemical composition of the steel alloy 1.3505, given in table 1. Following [27] and [28], mechanical and thermal data such as Poisson's ratio or Young's modulus are computed depending on the temperature. Moreover, the martensitic start temperature is determined at 185 °C. The volume fractions after phase transformation and the needle-like microstructure are determined as approximately 87.2% martensite and 12.8% retained austenite.

Table 1: Chemical composition of the steel alloy 1.3505 for material data generation using JMatPro.

Chemical composition [wt%]	**C**	**Si**	**Mn**	**P**	**S**	**Cr**	**Mo**	**Fe**
1.3505 (DIN 100Cr6) [29]	0.99	0.25	0.35	0.025	0.015	1.475	0.1	balance

3 NUMERICAL ANALYSIS OF MESOSCOPIC RESIDUAL STRESSES DUE TO PHASE TRANSFORMATION ON THE MICROSCALE

Based on data obtained from the experimental and numerical investigations regarding the macroscale presented in section 2, the numerical model originally proposed in [8] is summarized. For details and further illustrations of the workflow, it is referred to the mentioned reference. It accounts for the austenite-to-martensite (A-M) phase transformation during rapid cooling in water and investigates the resulting residual stress distribution on a mesoscopic level, see section 3.4. Therefore, Multi-Phase-Field (MPF) simulations in combination with Finite Element (FE) simulation are utilized and applied to the investigated material 1.3505 (DIN 100Cr6).

3.1 Multi-Phase-Field theory

The Multi-Phase-Field (MPF) model, which is used to describe the austenite-to-martensite (A-M) phase transformation during rapid cooling, was introduced by [9], [10] and [11], among others. An open source implementation is available, see [30]. A general free energy description is utilized that distinguishes between different physical phenomena. In a domain Ω, the free energy density F can be divided into the interfacial energy density f^{intf}, the chemical energy density f^{chem} and the elastic energy density f^{elast}, thus

$$\begin{aligned} F &= \int_\Omega f^{\text{intf}} + f^{\text{chem}} + f^{\text{elast}} \,\mathrm{d}\Omega\,, \\ f^{\text{intf}} &= \sum_{\alpha,\beta=1,\dots,N,\alpha\neq\beta} \frac{4\sigma_{\alpha\beta}}{\eta_{\alpha\beta}} \left[-\frac{\eta_{\alpha\beta}^2}{\pi^2} \nabla\phi_\alpha \cdot \nabla\phi_\beta + \phi_\alpha\phi_\beta \right] , \\ f^{\text{chem}} &= \sum_{\alpha=1,\dots,N} h(\phi_\alpha) f_\alpha(c_\alpha^i) + \tilde{\mu}^i (c^i - \sum_{\alpha=1,\dots,N} \phi_\alpha c_\alpha^i)\,, \\ f^{\text{elast}} &= \frac{1}{2} \Big[\sum_{\alpha=1,\dots,N} h(\phi_\alpha) (\boldsymbol{\varepsilon}_\alpha - \boldsymbol{\varepsilon}_\alpha^* - c_\alpha^i \boldsymbol{\varepsilon}_\alpha^i) : \mathbb{C}_\alpha : (\boldsymbol{\varepsilon}_\alpha - \boldsymbol{\varepsilon}_\alpha^* - c_\alpha^j \boldsymbol{\varepsilon}_\alpha^j) \Big] . \end{aligned} \tag{1}$$

The phase-field parameter for an individual phase α is labeled as ϕ_α. The diffusion equation

$$\dot{\phi}_\alpha = \sum_{\beta=1,\dots,N} \frac{\pi^2 \mu_{\alpha\beta}}{8\eta N} \Big(\frac{\partial F}{\partial \phi_\beta} - \frac{\partial F}{\partial \phi_\alpha} \Big) \tag{2}$$

controls its evolution. Additional physical quantites occurring in the stated formula are listed in table 2.

3.2 Homogenization of eigenstrains in one martenstitic grain

Rapid cooling from forging heat triggers the formation of martensite when reaching the martensitic start temperature. Each grain changes separately due to orientation and evolving martensite variant, i.e. it is necessary to take different martensitic variants into account, see [31]. Moreover, the different lattice types for austenite and martensite have to be embedded. Austenite consists of face-centered cubic unit cells, but diffusionless phase

Table 2: Quantities governing the MPF model in equations (1) and (2).

i, j	components
α, β	identifier of phase-fields
N	total number of phase-fields
$\sigma_{\alpha\beta}$	energy of the interface between phase-fields α and β
$\eta_{\alpha\beta}$	interface width between phase-fields α and β
$f_\alpha(c_\alpha^i)$	chemical potential for phase-field α
c_α^i	concentration of component i in phase-field α
$\tilde{\mu}^i$	generalized chemical potential or diffusion potential as Lagrange multiplier for satisfying the balance of mass for each component ($c^i = \sum_{\alpha=1,\dots,N} \phi_\alpha c_\alpha^i$)
$\boldsymbol{\varepsilon}_\alpha$	total strain of phase-field α
$\boldsymbol{\varepsilon}_\alpha^*$	eigenstrain of phase-field α
$\boldsymbol{\varepsilon}_\alpha^i$	strain of component i in phase-field α
$\mathbb{C}_\alpha$	elasticity tensor of phase-field α
$h(\phi_\alpha)$	polynomial function fulfilling $h(1) = 1$ and $h(0) = 0$ with $h(\phi_\alpha) = \phi_\alpha$
$\mu_{\alpha\beta}$	effective interfacial mobility between phase-fields α and β

transformations result in martensite with body-centered tetragonal lattice structure. Such shifting can be expressed by the socalled Bain-groups, which enable to describe in total all 24 variants of martensite forming from austenite. It is to be noticed that up to now shearing and rotation are neglected, such that only three variants are included in this model, see figure 2a.

In a first step, this microscopic transformation in one grain is analyzed. Therefore, a MPF simulation with following initial configuration is done. A cube made from austenite with three martensitic nulcei is taken into account. Each nucleus represents one of the three considered variants, I, II or III. Transversally isotropic eigenstrain tensors representing the volume change during transformation are applied according to the variant number, which are given by

$$\begin{aligned} \operatorname{diag} \boldsymbol{\varepsilon}_{\mathrm{I}}^* &= [-0.2 \quad 0.12 \quad 0.12]\,, \\ \operatorname{diag} \boldsymbol{\varepsilon}_{\mathrm{II}}^* &= [\ 0.12 \quad -0.2 \quad 0.12]\,, \\ \operatorname{diag} \boldsymbol{\varepsilon}_{\mathrm{III}}^* &= [\ 0.12 \quad 0.12 \quad -0.2]\,. \end{aligned} \tag{3}$$

Due to high temperatures, it is possible to consider the occurring transformation in the framework of small strains. The simulation follows the principle of minimizing the total energy in the system and results in a microscopic laminate consisting of two of the three variants, shown in figure 2b. To obtain information regarding the mesoscale and, in particular, the mechanical energy and mechanical driving force, a partial-rank one homogenization scheme is applied. It is described in [32], [33] and [34] and successfully applied to OpenPhase in [35]. Thus, the static equilibrium as well as strain compatibility condition at the interfaces are ensured. With that, the effective (homogenized) eigenstrain tensor can be calculated by application of a volume averaging scheme

$$\begin{aligned} \operatorname{diag} \overline{\boldsymbol{\varepsilon}}^*_{\mathrm{II,III}} &= [\ 0.12 \quad -0.04 \quad -0.04]\,, \\ \operatorname{diag} \overline{\boldsymbol{\varepsilon}}^*_{\mathrm{I,III}} &= [-0.04 \quad 0.12 \quad -0.04]\,, \\ \operatorname{diag} \overline{\boldsymbol{\varepsilon}}^*_{\mathrm{I,II}} &= [-0.04 \quad -0.04 \quad 0.12]\,. \end{aligned} \tag{4}$$

It is assumed that the volume fraction of each variant in the laminate equals 50%. Now, these tensors can be utilized for mesoscopic calculation, representing microscopic effects such as the internal laminate structure of martensitic grains.

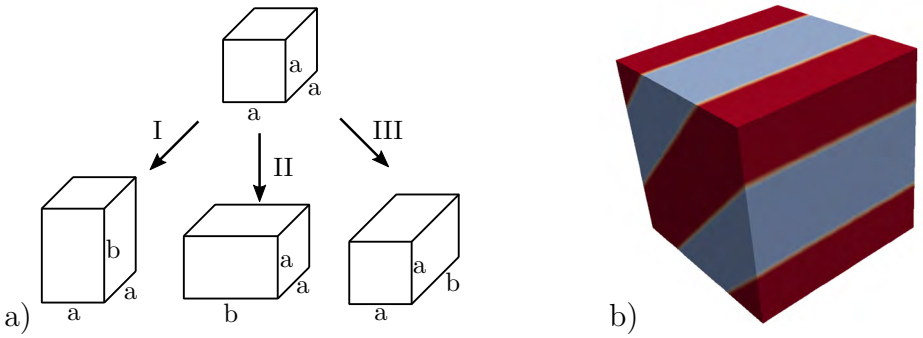

Figure 2: a) Three considered martensitic variants, cf. [31], with a_0 as edge length of an austenitic unit cell and a, b as edge length of a tetragonally transformed martensitic unit cell and b) laminate consisting of two variants of martensite, namely I+II or II+III or I+III.

3.3 Austenite-to-martensite phase transformation

The mesoscopic structure of steels such as 1.3505 (DIN 100Cr6) can be represented by a polycrystal, which can be obtained from a MPF model. Thus, a matrix with 24 arbitrarily placed nuclei is considered in a cube of edge length 121 grid points. Those nuclei differ by the orientations of their crystallographic lattice, which have been defined with help of a geodesic dome leading to overall isotropic orientation of the polycrystal. Applying a MPF simulation controlled by normal grain growth to the initial set up, which is stopped when the matrix has vanished completely, leads to an austenitic polycrystal of 24 grains, see figure 3a. Afterwards, this polycrystal is exposed to a linear mapping, which reduces the height to 50% of its initial value and thus describes the experimental upsetting, see section 2. Fulfilling volume preservation, the new grid has $171 \times 171 \times 61$ grid points, illustrated in figure 3b.

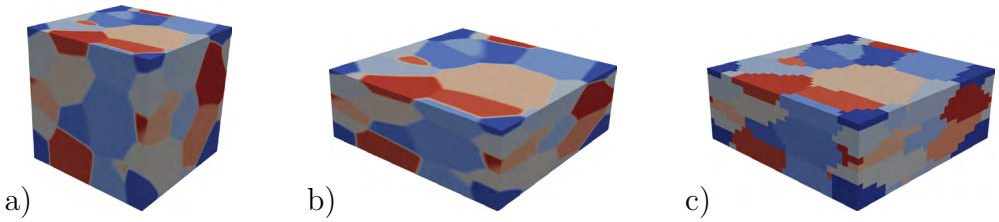

Figure 3: Polycrystal a) before and b) after deformation and c) after coarsening.

In a next step, the phase transformation itself has to be depicted. The volume fractions of austenite and martensite after transformation are considered as a result of the macroscopic experiments and simulations, cf. section 2. From initially 100% austenite, approximately 12.8% remain as retained austenite, while the other 87.2% of the volume undergo phase transformation to martensite. Analyzing the volume fractions of all 24 grains in comparison with the total volume, four grains are taken into account as a good fit to represent the retained austenite, since their combined volume equals exactly 12.8%. They are not taken into account for the transformation scheme, while the other 20 grains are considered to undergo transformation to martensite. At first, one of the effective eigenstrain tensors $\bar{\boldsymbol{\varepsilon}}_i^*$, cf. equation (4), is assigned arbitrarily to each considered grain. The set of all eigenstrain states for the 20 grains is given by

$$\boldsymbol{V} \;=\; \{\bar{\boldsymbol{\varepsilon}}_1^*, ..., \bar{\boldsymbol{\varepsilon}}_{20}^*\} \quad \text{for} \quad \bar{\boldsymbol{\varepsilon}}_i^* \in \{\overline{\boldsymbol{\varepsilon}}_{\mathrm{II,III}}^*\,, \overline{\boldsymbol{\varepsilon}}_{\mathrm{I,III}}^*\,, \overline{\boldsymbol{\varepsilon}}_{\mathrm{I,II}}^*\}\,. \tag{5}$$

Then, an iterative optimization procedure is applied grain by grain following the principle of minimizing the elastic energy f^{elast} in the system, which has been introduced in [8] as

$$\tilde{\boldsymbol{V}} \;=\; \arg\Big[\min_{\boldsymbol{V}}[f^{\mathrm{elast}}(\boldsymbol{V})]\Big]\,, \tag{6}$$

with $\tilde{\boldsymbol{V}}$ as optimized set of eigenstrain states leading to the minimized elastic energy. In relation to $\tilde{\boldsymbol{V}}$, a mesoscopic strain distribution $\boldsymbol{\varepsilon}^{\mathrm{MPF}}(\boldsymbol{x})$ is obtained, which stands for strains occurring in the A-M phase transformation in a polycrystal.

3.4 Residual stress calculation

All MPF models used here only consider elastic strains, such that the utilization of an elasto-plastic FE simulation is inevitable. The mechanical behavior is defined by an elasto-plastic material law with a von Mises yield criterion with exponential hardening, cf. [36]. In table 3 the used material parameters are given for austenite and martensite at the predefined martensitic start temperature of 185° C.

Table 3: Material parameters for austenite (A) and martensite (M) at temperature 185 °C: Youngs's modulus E in MPa and Poisson's ratio ν, initial yield strength y_0 in MPa, limiting yield strength y_∞ in MPa, parameter for exponential hardening δ, linear hardening parameter h in MPa.

	E in MPa	ν	y_0 in MPa	y_∞ in MPa	δ	h in MPa
A	186,610.988	0.301141	333.766	713.135	35	520
M	200,372.074	0.295635	2 609.125	3 057.886	20	500

Equation (7) describes how the mesoscopic strain distribution $\boldsymbol{\varepsilon}^{\mathrm{MPF}}(\boldsymbol{x})$ resulting from the optimal set of eigenstrain states $\tilde{\boldsymbol{V}}$, representing the strains resulting from the A-M phase transformation, is applied as driving force on finite element level. The strain state is incrementally assigned to the total strain field over a pseudo-time t, in which t^n and t^{n+1} stand for the last and actual time step, respectively,

$$\boldsymbol{\varepsilon}(\boldsymbol{u}, \boldsymbol{x}, t^{n+1}) \Leftarrow \boldsymbol{\varepsilon}(\boldsymbol{u}, \boldsymbol{x}, t^{n}) - \boldsymbol{\varepsilon}^{\mathrm{MPF}}(\boldsymbol{x}, t^{n+1})\,. \tag{7}$$

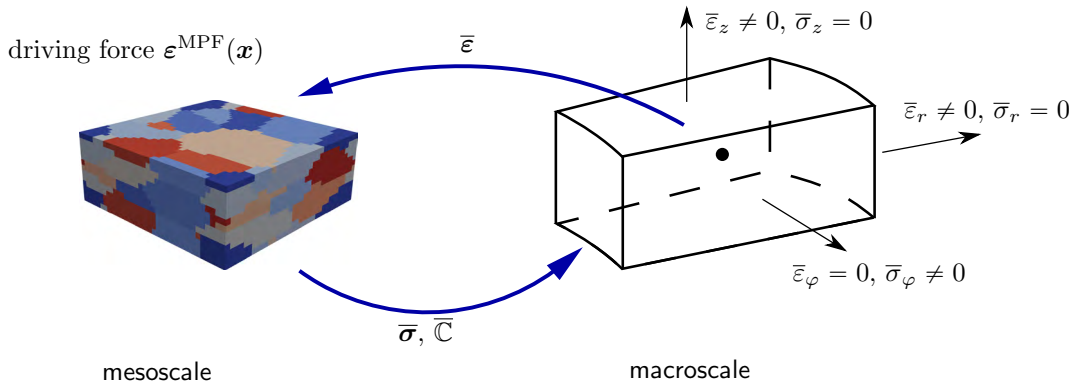

Figure 4: Two-scale boundary value problem for the incorporation of the strains $\boldsymbol{\varepsilon}^{\mathrm{MPF}}(\boldsymbol{x})$ in the FE-model. Macroscopic quantities are denoted by an overline.

For the incorporation of $\boldsymbol{\varepsilon}^{\mathrm{MPF}}(\boldsymbol{x})$ and the phase-field parameter ϕ, a one to one mapping of the grid points from OpenPhase to hexahedral finite elements is chosen. This voxel-like representation accounts for an element wise constant strain distribution. Furthermore, to obtain a better numerical performance, the MPF grid is coarsened by a factor of 5 to $35 \times 35 \times 13$ elements, cf. figure 3c. This discretization of the granular structure is utilized for a two-scale FE calculation, following e.g. [22] or [23]. On the macroscale, a section of the cylindrical specimen with the enforced boundary conditions is considered, see figure 4. There, r, φ and z indicate the radial direction, the tangential direction and the height, respectively. For the lower scale, i.e. mesoscale, the polycrystal with the mesoscopic strain distribution from the MPF simulation as driving force is used. This boundary value problem is solved at each macroscopic intergration point under application of periodic boundary conditions.

Figure 5a-c displays the radial and tangential stresses on the mesoscale as well as the mesoscopic axial stresses with respect to the height. During the simulation, no outer forces have been applied. Hence, these stress distribution can be interpreted as residual stresses instead of mechanically induced stress. The tangential stresses σ_φ are most relevant when investigating the durability or strength of a component, since those are the only stresses not enforced to be zero on average. Furthermore, it should be noticed that the other stress components, namely σ_r and σ_z, level out over the complete domain, since it holds $\bar{\sigma}_r = -0.424\,10^{-12} \approx 0$ and $\bar{\sigma}_z = -0.161\,10^{-11} \approx 0$. Additionally, the equivalent plastic strains, the von Mises stress and the phase distribution after transformation are shown in figure 5d-f. The retained austenite is presented as red islands in a martensitic matrix.

4 CONCLUSIONS

In this work, a model for the analysis of residual stresses on the mesoscale due to austenite-to-martensite phase transformation was introduced. Based on experiments and macroscopic Finite-Element (FE) simulations as well as predefined material data, a mesoscopic model was built. Elastic Multi-Phase-Field (MPF) models in combination with two-scale elasto-plastic FE simulation have been utilized. Based on mesoscopic stresses

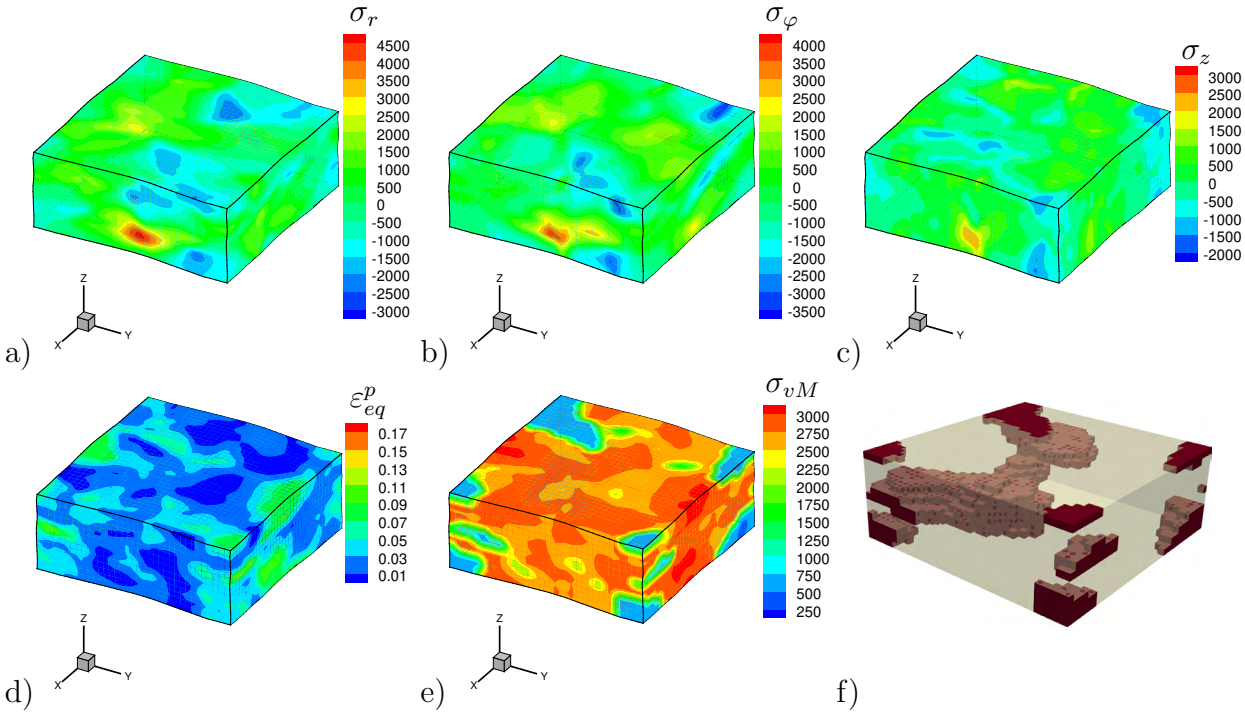

Figure 5: a) Radial stresses σ_r in MPa, b) tangential stresses σ_φ in MPa, c) axial stresses σ_z in MPa, d) equivalent plastic strains and e) von Mises stress in MPa. e) Phase distribution after transformation: red for austenite and yellow for martensite.

due to the austenite-to-martensite phase transformation on the microscale, the development of mesoscopic residual stresses due to phase transformation has been described.

In future steps, the MPF model for the laminates of one martenstitic grain should be revised to be more realistic. Moreover, the relaxation of the elastic energy to find a suitable eigenstrain distribution should be executed in a semi automated manner and the residual stress calculation with finite elements should involve the complete thermo-elasto-plastic cooling process. By validation of the results based on the interactions of the thermo-mechanical investigations on all scales, an improvement of the residual stress calculation and a prediction of targeted residual stress states should be enabled.

Acknowledgment: Funded by the Deutsche Forschungsgemeinschaft (DFG, German Research Foundation) - 374871564 (BE 1691/223-1, BR 5278/3-1, SCHR 570/33-1) within the priority program SPP 2013. The authors thank Prof. Dr.-Ing. Bernd-Arno Behrens, Dipl.-Ing. Alexander Chugreev and Christoph Kock from IFUM (Institute of Forming Technology and Machines) at the Leibniz Universität Hannover as well as their colleagues Dr.-Ing. Rainer Niekamp and Mohammad Sarhil from Universität Duisburg-Essen for the inspiring collaboration. Furthermore, the authors thank Prof. Dr. Ingo Steinbach and Dr. Oleg Shchyglo from ICAMS (Interdisciplinary Center for Advanced Materials Simulation) at the Ruhr-Universität Bochum for their scientific support.

REFERENCES

[1] A.E. Tekkaya, J. Gerhardt, and M. Burgdorf. Residual Stresses in Cold-Formed Workpieces. *Manufacturing Technology*, 34:225–230, 1985.

[2] M.P. Mungi, S.D. Rasane, and P.M. Dixit. Residual stresses in cold axisymmetric forging. *Journal of Materials Processing Technology*, 142(1):256–266, 2003.

[3] D. von Mirbach. Hole-drolling method for residual stress measurement - consideration of elastic-plastic material properties. *Material Science Forum*, 768-769:174–181, 2014.

[4] W. Seidel. *Werkstofftechnik - Werkstoffe, Eigenspannungen, Prüfung, Anwendungen*. Hanser Verlag, 7 edition, 2007.

[5] B.-A. Behrens and J. Schrödter. Numerical Simulation of Phase Transformation during the Hot Stamping Process. In *Thermal Process Modeling: Proceedings from the 5th International Conference on Thermal Process Modeling and Computer Simulation*, pages 179–190, 2014.

[6] E. Macherauch, H. Wohlfahrt, and U. Wolfstied. *Härterei-Technische Mittelungen - Zeitschrift für Werkstoffe, Wärmebehandlung, Fertigung*, 28(3):201–211, 1973.

[7] M.A.S. Torres and H.J.C. Voorwald. An evaluation of shot peening, residual stress and stress relaxation on the fatigue life of ASIS 4340 steel. *International Journal of Fatigue*, 24:877–886, 2002.

[8] B.-A. Behrens, J. Schröder, D. Brands, L. Scheunemann, R. Niekamp, M. Sarhil, S. Uebing, and C. Kock. Experimental and Numerical Investigations of the Development of Residual Stresses in Thermo-Mechanically Processed Cr-Alloyed Steel 1.3505. *Metals*, 9(4):480 (28 pages), 2019.

[9] I. Steinbach, F. Pezzolla, B. Nestler, M. Seeßelberg, R. Prieler, G.J. Schmitz, and J.L.L. Rezende. A phase field concept for multiphase systems. *Physica D: Nonlinear Phenomena*, 94(3):135–147, 1996.

[10] J. Tiaden, B. Nestler, H.J. Diepers, and I. Steinbach. The multiphase-field model with an integrated concept for modelling solute diffusion. *Physica D: Nonlinear Phenomena*, 115(1):73–86, 1998.

[11] I. Steinbach and F. Pezzolla. A generalized field method for multiphase transformations using interface fields. *Physica D: Nonlinear Phenomena*, 134(4):385–393, 1999.

[12] I. Steinbach and M. Apel. Multi phase field model for solid state transformation with elastic strain. *Physica D*, 217:153–160, 2006.

[13] I. Steinbach. Phase-field models in materials science. *Modelling and Simulation in Materials Science and Engineering*, 17:073001 (31 pages), 2009.

[14] D. Schneider, S. Schmid, M. Selzer, T. Böhlke, and B. Nestler. Small strain elasto-plastic multiphase-field model. *Computational Mechanics*, 55:27–35, 2015.

[15] D. Schneider, F. Schwab, E. Schoof, A. Reiter, C. Herrmann, M. Selzer, T. Böhlke, and B. Nestler. On the stress calculation within phase-field approaches: a model for finite deformations. *Computational Mechanics*, 60:203–217, 2017.

[16] D. Schneider, E. Schoof, O. Tschukin, A. Reiter, C. Herrmann, F. Schwaab, M. Selzer, and B. Nestler. Small strain multiphase-field model accounting for configurational forces and mechanical jump conditions. *Computational Mechanics*, 61:277–295, 2018.

[17] E. Schoff, D. Schneider, N. Streichhan, T. Mittnacht, M. Selzer, and B. Nestler. Multiphase-field modeling of martensitic phase transformation in a dual-phase microstructure. *International Journal of Solids and Structures*, 134:181–194, 2017.

[18] C. Herrmann, E. Schoof, D. Schneider, F. Schwab, A. Reiter, M. Selzer, and B. Nestler. Multiphase-field model of small strain elasto-plasticity according to the mechanical jump conditions. *Computational Mechanics*, 62(6):1399–1412, 2018.

[19] E. Schoof, C. Herrmann, N. Streichhan, M. Selzer, D. Schneider, and B. Nestler. On the multiphase-field modeling of martensitic phase transformation in dual-phase steel using J2-viscoplasticity. *Modelling and Simulation in Materials Science and Engineering*, 27:025010 (24 pages), 2019.

[20] R. Schmitt, C. Kuhn, R. Müller, and K. Bhattacharya. Crystal Plasticity and Martensitic Transformations - A Phase Field Approach. *Technische Mechanik*, 34:23–28, 2014.

[21] R. Schmitt. *A Phase Field Model for Martensitic Transformations and Crystal Plasticity*. PhD thesis, TU Kaiserslautern, 2015.

[22] C. Miehe, J. Schröder, and J. Schotte. Computational homogenization analysis in finite plasticity. Simulation of texture development in polycrystalline materials. *Computer Methods in Applied Mechanics and Engineering*, 171(3-4):387–418, 1999.

[23] J. Schröder. A numerical two-scale homogenization scheme: the FE^2-method. In *Plasticity and Beyond - Microstructures, Crystal-Plasticity and Phase Transitions (CISM Lecture Notes 550, Eds. J. Schröder, K. Hackl)*, pages 1–64. Springer, 2014.

[24] D. Brands, D. Balzani, L. Scheunemann, J. Schröder, H. Richter, and D. Raabe. Computational modeling of dual-phase steels based on representative three-dimensional microstructures obtained from EBSD data. *Archive of Applied Mechanics*, 86:575–598, 2016.

[25] C. Simsir and C.H. Gür. 3D FEM simulation of steel quenching and investigation of the effect of asymmetric geometry on residual stress distribution. *Journal of Materials Processing Technology*, 207:211–221, 2008.

[26] JMatPro. Practical software for materials properties, https://www.sentesoftware.co.uk/jmatpro. August 2018.

[27] N. Saunders, U.K.Z. Guo, X. Li, A.P. Miodownik, and J.-P. Schillé. Using JMatPro to Model Materials Properties and Behavior. *JOM*, 55(12):60–65, 2003.

[28] Z. Guo, N. Saunders, J.-P. Schillé, and A.P. Miodownik. Material properties for process simulation. *Materials Science and Engineering: A*, 1-2:7–13, 2009.

[29] DIN EN ISO 683-17. Heat-treated steels, alloy steels and free-cutting steels - Part 17: Ball and roller bearing steels. Technical report, Beuth-Verlag, 2014.

[30] OpenPhase. http://www.openphase.de/. August 2018.

[31] K. Bhattacharya. *microstructure of martensite: why it forms and how it gives rise to the shape-memory effect*. Oxford University Press, Oxford, 2003.

[32] J. Mosler, O. Shchyglo, and H. Montazer Hojjat. A novel homogenization method for phase field approaches based on partial rank-one relaxation. *Journal of the Mechanics and Physics of Solids*, 68:251–266, 2014.

[33] A. Bartels and J. Mosler. Efficient variational constitutive updates for Allen-Cahn-type phase field theory coupled to continuum mechanics. *Computer Methods in Applied Mechanics and Engineering*, 317:55–83, 2017.

[34] B. Kiefer, T. Furlan, and J. Mosler. A numerical convergence study regarding homogenization assumptions in phase field modeling. *International Journal for Numerical Methods in Engineering*, 112:1097–1128, 2017.

[35] M. Sarhil. Constitutive Relations and Homogenization Assumptions in Phase-Field Models with Elasticity: Martensite Transformation as an Example. Master's thesis, Universität Duisburg-Essen and Ruhr-Universität Bochum, Essen, 2018.

[36] C. Miehe. *Kanonische Modelle Multiplikativer Elasto-Plastizität - Thermodynamische Formulierung und Numerische Implementation*. Forschungs- und Seminarberichte aus dem Bereich der Mechanik der Universität Hannover, Hannover, 1992.